CHAPTER 5

DAMAGE DETECTION OF STRUCTURES VIA NEURAL NETWORKS

5.1   Introduction

The damage of a structure is conventionally assessed from observed dynamic responses by detecting changes in the modal parameters of the structure. The concept underlying such an approach is that damage to a structure reduces its natural frequencies, increases the modal damping, and changes the modal shapes. In early research, structural damage detection methods use natural frequencies as damage indicator. However, the frequencies are not spatially specific and are not very sensitive to damage so that its application is limited. Since mode shapes can provide much more information than natural frequencies, many studies have concentrated their efforts on damage detection with mode shapes information.

Recently, structural damage identification based on vibration monitoring techniques has paid much attention. Various damage identification algorithms have been developed for dealing with three key problems, i.e., detection of the presence of damages, detection of the structural damage locations, and estimation of the damage extents. For the problems stated above, most of the existing methods can be thought of as a two-stage algorithm in which damage locations are detected at first, and then damage extents are estimated. Generally, the first step may be more

important, but probably more difficult.

Due to the features of robustness, fault tolerance, and powerful computing ability, the model of artificial neural networks becomes a promising tool in solving civil engineering problems. Masri *et al.* [52] has demonstrated in their study that neural networks are a powerful tool for the identification of systems typically encountered in the structural dynamics field. Some researches have investigated and proven the suitability and capabilities of ANNs for damage detection purposes. Consequently, the ANNs are also employed to develop the damage detection methods in this work.

By using the modal data extracted from the structural responses via the aforementioned ANNSI model in Chapter 4, the damage locations and extents in the structure can be identified and evaluated. A two-stage damage assessment approach for building structures is used in this study. The first stage focuses on identifying the damage locations of the damaged structure by using ANNs and the second stage works on the estimation of the damage extents.

5.2   Damage Detection By Using The UFN Model

Based on recent developments in measuring and data analyzing techniques, modal data (such as natural frequencies and mode shapes) of a structural system can easily be obtained through utilizing system identification procedure. Therefore, the damage detection approach has been developed on the basis of the available natural frequencies and mode shapes of the structures.

5.2.1   Index for Damage Localization

For an undamaged structure, the modal characteristics are described by the following eigenvalue equation:

$$[\mathbf{K} - l_i\mathbf{M}]\mathbf{f}_i = 0 \qquad \text{for } i = 1,..., N \tag{5.1}$$

where l_i is the ith modal eigenvalue which presents the square of the natural frequency of the structure; $\mathbf{f}_i$ is the ith eigenvector which presents the mode shape of the structure; $\mathbf{K}$ and $\mathbf{M}$ are symmetric system stiffness and mass matrices, respectively.

Generally, the damage of a structure is assumed to be the reduction of stiffness but not the loss of mass in structural elements, then the eigenvalue equation for such a damaged structure becomes

$$[(\mathbf{K} - \Delta\mathbf{K}) - (l_i - \Delta l_i)\mathbf{M}](\mathbf{f}_i - \Delta\mathbf{f}_i) = 0 \tag{5.2}$$

Assume the system stiffness matrix is the combination of individual member stiffness matrices. The change in stiffness matrix due to damage then be expressed as

$$\Delta\mathbf{K} = \sum_{e=1}^{N_d} a_e \mathbf{k}_e \tag{5.3}$$

where $\mathbf{k}_e$ is the individual stiffness matrix for the eth element; N_d is the total number of damaged elements in the structure; and a_e, which is within the range between 0 and 1, is the coefficient defining a fractional change of the eth elemental stiffness matrix. Therefore, the index, a, which is damage extent-dependent, makes estimation on the damage extent and the suffix, e, which is damage location-dependent, offers the information about the location of the damage. In the

case of $a_e = 0$, the eth structural element is not damaged. When $a_e = 1$, in contrast,
it means that the eth structural element is totally damaged. Accordingly, the
problems of locating the damage site and evaluating the damage extent are focus on
identifying the index e and computing the corresponding value of a_e.

Expand equation (5.2) and neglect the higher order terms of Δ yields

$$-\Delta \mathbf{K} \mathbf{f}_i + \Delta l_i \mathbf{M} \mathbf{f}_i - \mathbf{K} \Delta \mathbf{f}_i + l_i \mathbf{M} \Delta \mathbf{f}_i = 0 \qquad (5.4)$$

Pre-multiply equation (5.4) with $\mathbf{f}_i^T$, the change in eigenvalue is then expressed by

$$\Delta l_i = \frac{\mathbf{f}_i^T \Delta \mathbf{K} \mathbf{f}_i}{\mathbf{f}_i^T \mathbf{M} \mathbf{f}_i} \qquad (5.5)$$

This equation expresses the relationship between the structural damage and the
change in eigenvalue of the damaged structure. The eigenvalue change is direct
proportion to the extent of damage.

Now Substitute $\Delta \mathbf{K}$ with equation (5.3), equation (5.5) becomes

$$\Delta l_i = \frac{\mathbf{f}_i^T \sum_{e=1}^{N_d} a_e \mathbf{k}_e \mathbf{f}_i}{\mathbf{f}_i^T \mathbf{M} \mathbf{f}_i} \qquad (5.6)$$

It is seen that the change in eigenvalue is damage location-dependent (the index, e)
as well as damage extent-dependent (the index, a).

Subsequently, the relationship between the structural damage and the change in
eigenvector is derived. Pre-multiply equation (5.4) with the transpose of the jth
eigenvector, $\mathbf{f}_j^T$, and use the relationship, $\mathbf{f}_j^T \mathbf{K} = l_j \mathbf{f}_j^T \mathbf{M}$, which leads to the
following equation:

$$(\boldsymbol{l}_j - \boldsymbol{l}_i)\boldsymbol{f}_j^T \mathbf{M}\Delta \boldsymbol{f}_i = -\boldsymbol{f}_j^T \Delta \mathbf{K} \boldsymbol{f}_i \qquad (5.7)$$
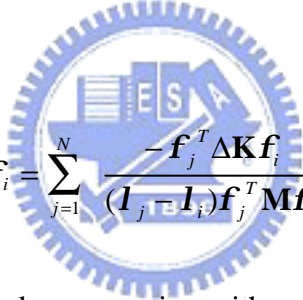
where $\Delta \boldsymbol{f}_i$ is assumed to be a linear combination of the mode shapes [99], i.e.

$$\Delta \boldsymbol{f}_i = \sum_{k=1}^{N} c_{ik} \boldsymbol{f}_k \qquad (5.8)$$

Substitute equation (5.8) into equation (5.7), and introduce the orthogonal property, equation (5.7) is rearranged as

$$c_{ij} = \frac{-\boldsymbol{f}_j^T \Delta \mathbf{K} \boldsymbol{f}_i}{(\boldsymbol{l}_j - \boldsymbol{l}_i)\boldsymbol{f}_j^T \mathbf{M} \boldsymbol{f}_j} \qquad (5.9)$$

Impose equation (5.9) onto equation (5.7), the expression show the change in ith eigenvector of the system.

$$\Delta \boldsymbol{f}_i = \sum_{j=1}^{N} \frac{-\boldsymbol{f}_j^T \Delta \mathbf{K} \boldsymbol{f}_i}{(\boldsymbol{l}_j - \boldsymbol{l}_i)\boldsymbol{f}_j^T \mathbf{M} \boldsymbol{f}_j} \boldsymbol{f}_j \qquad (5.10)$$

Again substituting $\Delta \mathbf{K}$ in the above equation with equation (5.3) yields

$$\Delta \boldsymbol{f}_i = \sum_{j=1}^{N} \frac{-\boldsymbol{f}_j^T \sum_{e=1}^{N_d} \boldsymbol{a}_e \mathbf{k}_e \boldsymbol{f}_i}{(\boldsymbol{l}_j - \boldsymbol{l}_i)\boldsymbol{f}_j^T \mathbf{M} \boldsymbol{f}_j} \boldsymbol{f}_j \qquad (5.11)$$

This equation, as equation (5.6), also shows that the change in eigenvector is damage location-dependent as well as damage extent-dependent. It is clear that equations (5.6) and (5.11) show the expression of changes in modal values and vectors, respectively. The changes in modal values and vectors are direct proportion to the stiffness change.

Finally, suppose single damage or multiple damages with similar severity (i.e. all $\boldsymbol{a}_e$, $e=1\sim N_d$, are identical) exist in the structure. With this assumption, the

expression for the change in the ith modal vector divided by the changes in the jth

modal value (i.e. divide equation (5.11) by equation (5.6)) can be obtained as follow:

$$\frac{\Delta f_i}{\Delta l_j} = \frac{\displaystyle\sum_{j=1}^{N} \frac{-f_j^T \sum_{e=1}^{N_d} k_e f_i}{(l_j - l_i) f_j^T M f_j} f_j}{\dfrac{f_j^T \sum_{e=1}^{N_d} k_e f_j}{f_j^T M f_j}} \tag{5.12}$$

Explicitly, the term, a, that represents the extent of the damage is eliminated.

Consequently, equation (5.12) depends on damage location only and the term on the

left-hand side, termed Damage Localization Feature (DLF) in this work, can be used

as an indicator for identifying the location of structural damage.

According to equation (5.12), the location of damage to a structure is dependent

only on the ratio of change in modal vectors and modal values, and can be identified

by matching the measured damage localization feature and the analytical damage

localization feature. This kind of problem solving process may be categorized as the

technique of pattern recognizing. And the unsupervised neural network model had

been widely applied and approved an efficient tool for the problem of pattern

recognition [48].

5.2.2   UFN for the Damage Detection of Structures

In the studies of damage detection that based on certain damage indices or

features, two main approaches are usually adopted to deal with the detection or

diagnosis process. One computed the discrepancy between the measured (or real)

damage index and the FEM-based analytical damage index for all potential damage

states to a structure. The case with the smallest discrepancy represents the current state for the structure [23, 100]. The other optimizes the specified objective function in which the measured information is included to search for the possible damage state [31]. Accordingly, no matter what approach is adopted, the key point of damage detection is how to rapidly and correctly identify the possible damage state according to the measured data. Therefore, one can establish the damage features for every possible damage state via the analytical FEM. When the measured damage feature is available from measurement, the damage state can then be identified through finding the same or most similar damage features. In most previous methods, the damage case with the smallest discrepancy between the measured and analytical damage features is selected to be the possible damage state on the structure. However, the identification of damage state basing on certain measured damage features is an inverse problem; two similar but different damage scenarios could possibly result in similar measured damage features. The relationship from the damage features to the damage state should be fuzzy but not crisp. Therefore, the damage cases with sufficient degree of 'similarity' between the measured and analytical damage features are selected as candidates to identify the damage state on the structure.

Note that, equation (5.12) was derived based on two assumptions: first, the higher order terms of Δ in equation (5.2) were neglected; second, the damage extents for multiple damages were identical when imposing equation (5.3) on equations (5.6) and (5.11). A consequence was made according to equation (5.12) that the damage location is depended only on $\dfrac{\Delta \boldsymbol{f}_i}{\Delta \boldsymbol{l}_j}$. That means, no matter what the damage extents are, $\dfrac{\Delta \boldsymbol{f}_i}{\Delta \boldsymbol{l}_j}$ is invariant for the same damage class (i.e. different

damage extent but same damage location). However, basing on the aforementioned
two assumptions, the actual computed values, $\dfrac{\Delta \boldsymbol{f}_i}{\Delta \boldsymbol{l}_j}$, will no longer be identical for a
specific damage class. For example, the respectively computed values, $\dfrac{\Delta \boldsymbol{f}_i}{\Delta \boldsymbol{l}_j}$, for the
damage occurred at the 1st story with 10% and 20% damage extent will lead to a
discrepancy between each other. The higher the difference in damage extent is, the
more the discrepancy. Meanwhile, for the example of multiple damages, such as the
damage occurred at the 1st and 2nd story with 10% and 20% damage extent, the
computed $\dfrac{\Delta \boldsymbol{f}_i}{\Delta \boldsymbol{l}_j}$ will also be different to that of the damage occurred at the same
stories but with 20% and 10% damage extent. Even though, one can find out from
the example (presented in section 5.2.4) that the DLF is still an effective feature for
determining the damage location. Accordingly, the process of using DLF to find the
damage location is more like pattern recognition than functional mapping.
Consequently, instead of the most utilized supervised neural network (which is
powerful for the functional mapping problems) in the related studies on damage
detection or health motoring, this study employs an unsupervised-typed neural
network model, the Unsupervised Fuzzy Neural Network (UFN) reasoning model, to
implement the damage localization process.

Together with the theories of DLF and the UFN reasoning model introduced in
section 3.3, this study makes use of the DLF as the input variables and the existence
of the damage site as the output vector for the UFN. Basing on the analytical model,
the Analytic Damage Localization Feature (ADLF) for various possible damage
cases can be calculated in advance to construct an ADLF *instance base*. With proper
deployment of sensors, the vibration signals of the structure can be easily measured
through ambient, free, or forced vibration tests, and the modal parameters can also

be generated through the ANNSI model. When the modal parameters of the structure are available, the damage location can then be located by matching the Measured Damage Localization Feature (MDLF) with the ADLF through the UFN reasoning.

5.2.3 Input-Output Patterns for the Neural Network

For each damage case, the ADLF can be derived using the left-hand-side of equation (5.12). For the UFN, the ADLF is treated as input variable of the neural network. Moreover, the output vector for the UFN represents the condition of the structural elements. Herein, binary value is adopted to represent the condition of the structural element. If the element is damaged, the value is set to be 1 to the associate element; otherwise, the value is set to be 0 to indicate an undamaged element. An example is presented in the next section to examine the feasibility of the proposed approach.
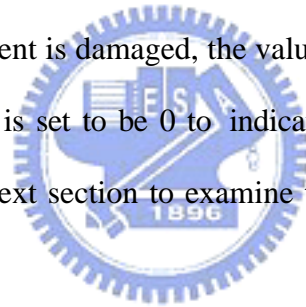
5.2.4 Example   Damage Detection of a Five-Story Shear Frame

A Numerical example, a five-story shear frame structure, is presented herein to investigate the feasibility of the proposed damage detection procedures. The structural parameters for each floor are set to be the same, i.e. the mass m_i=2 kg and the stiffness k_i=1500 N/m (i=1 to 5).

Simulated damage cases

In this example, the damage cases are simulated by the reduction of story stiffness of the 1st, 2nd, or 3rd story. Both single-site damage cases and multiple-site damage cases are discussed. Table 5.1 shows the characterizations of the simulated damage cases. Notably, the symbols Dam_k_i ($i = 1 \sim 3$) in Table 5.1 denote that the damage results in reduction of stiffness of k_i at single site (Case 1 to 60). Similarly, the symbols $Dam\_k_i \& k_j$ ($i \neq j$) mean that the damages result in reduction of stiffness of k_i and k_j at multiple sites (Case 61 to 132). The modal parameters of the undamaged and damaged cases are obtained through the analytical model.

Table 5.1 Characterizations of simulated damage cases

Damage class	Damage level	No. of damage case
Dam_k_1	2%~40% (every 2%)	Case 1~20
Dam_k_2	2%~40% (every 2%)	Case 21~40
Dam_k_3	2%~40% (every 2%)	Case 41~60
$Dam\_k_1 \& k_2$	5%~30% for k_1 (every 5%) 5%~30% for k_2 (every 5%)	Case 61~96
$Dam\_k_1 \& k_3$	5%~30% for k_1 (every 5%) 5%~30% for k_3 (every 5%)	Case 97~132

DLF of the numerical model

Figures 5.1 to 5.6, respectively, diagrammatically show the DLF for each simulated damage class listed in Table 5.1. As mentioned previously, the DLF depends on the damage location only. Consequently, the DLFs, shown in Figures 5.1

and 5.2 for the same damage class but with different damage levels, are almost the same. Moreover, Figures 5.2 to 5.6 depict that the DLF for different damage classes are distinguishable.

It is interested to mention that, although the DLFs for Dam_k_3 and $Dam\_k_1\&k_3$ class (Figures 5.4 and 5.6) are distinguishable, there exists certain degree of similarity between each other. This outcome is rational because these two damage classes are both damaged in the stiffness k_3.
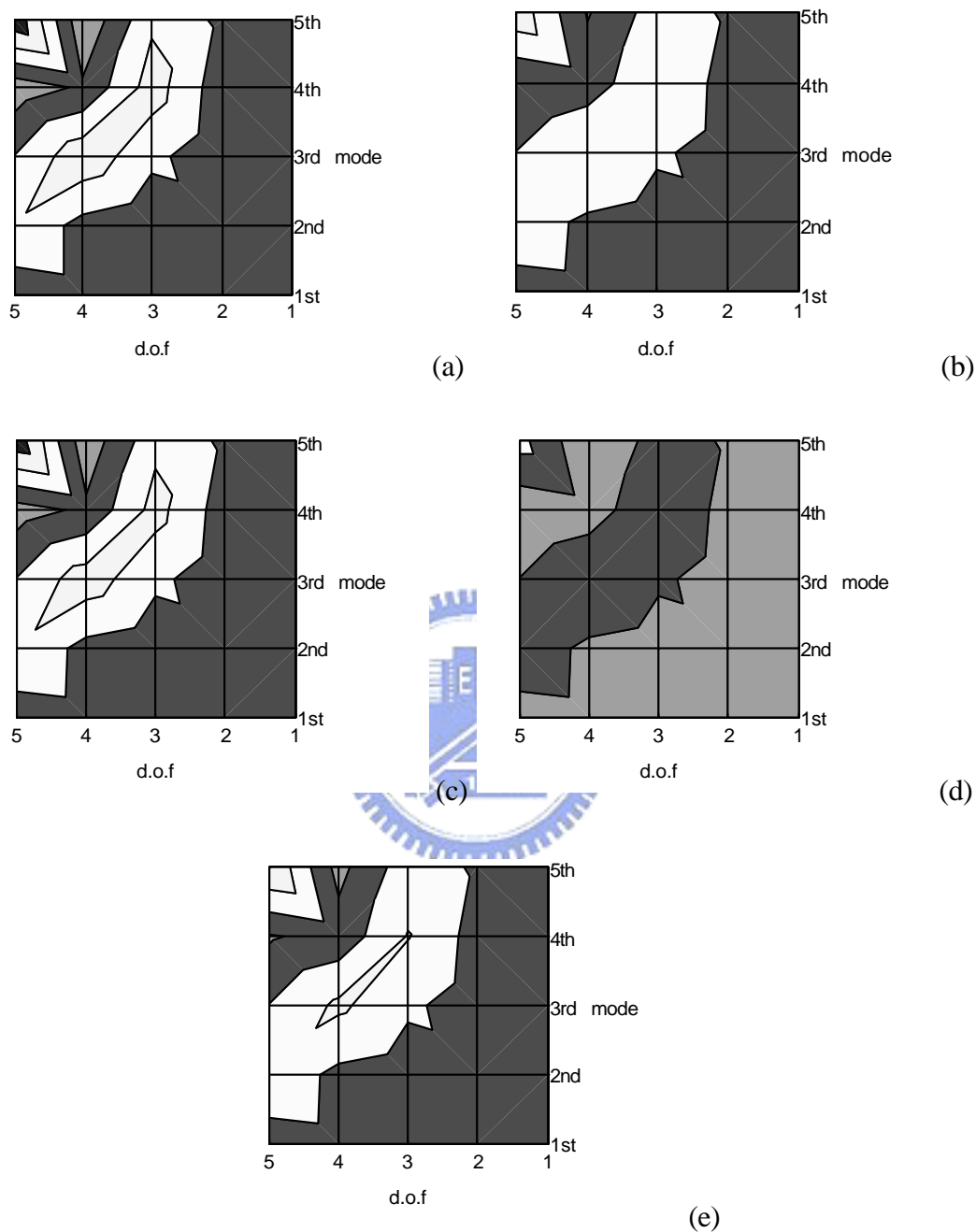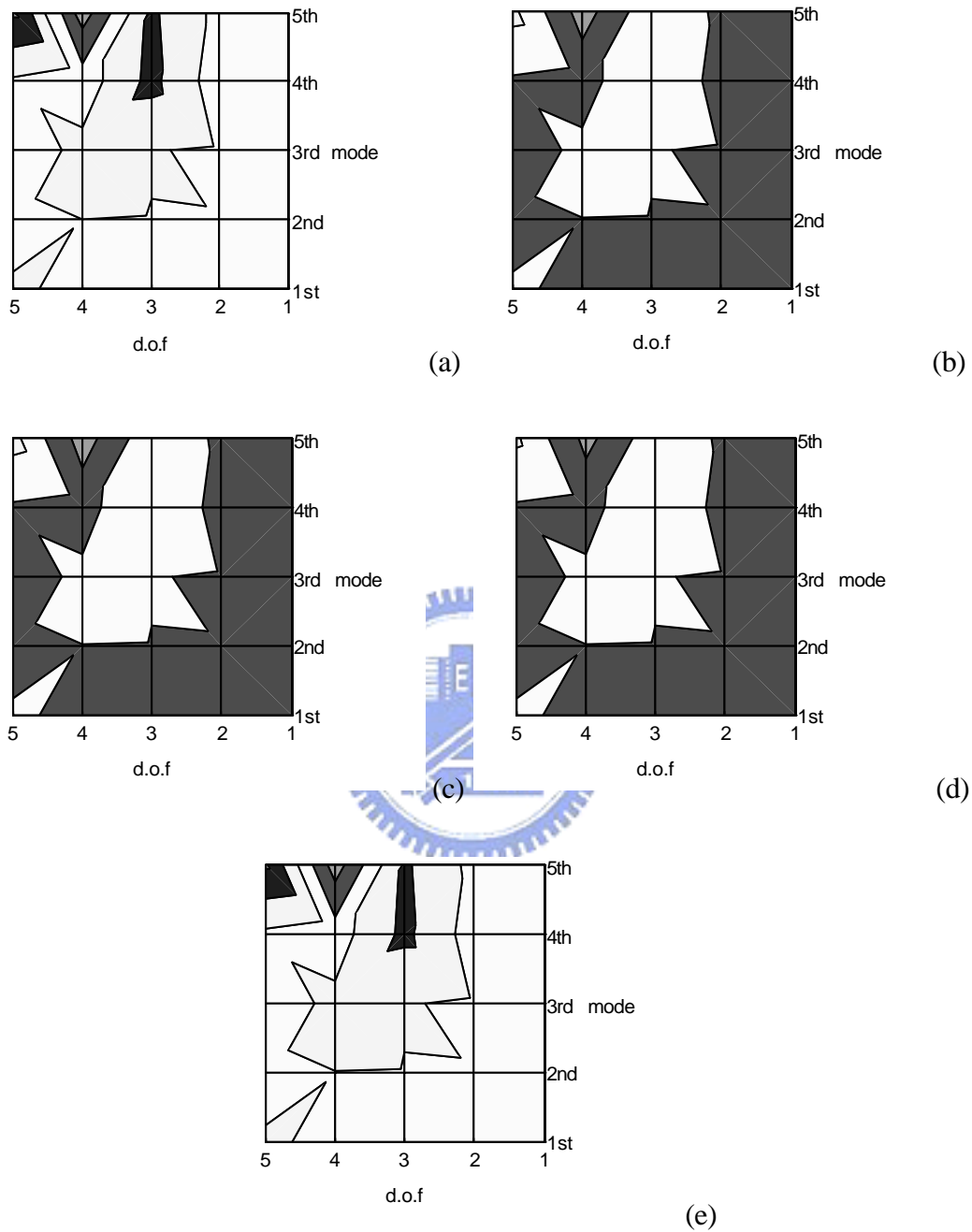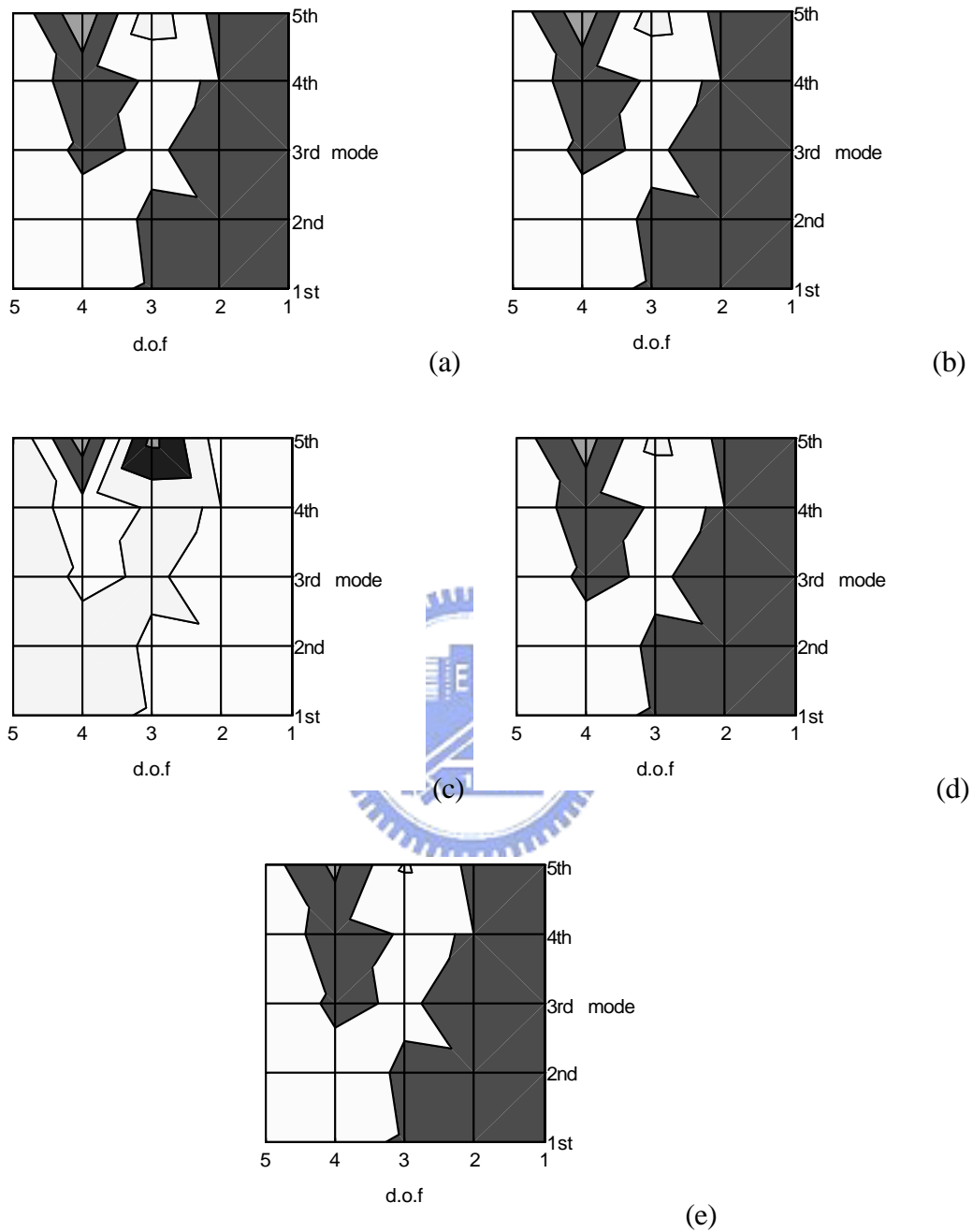
Figure 5.1 Plots of the DLF for the *Dam_k*₁ class with 20% damage extent

((a) to (e) are the plots of the DLF which are obtained by dividing the changes in the

modal vector to the changes in the 1st to 5th modal values, respectively)
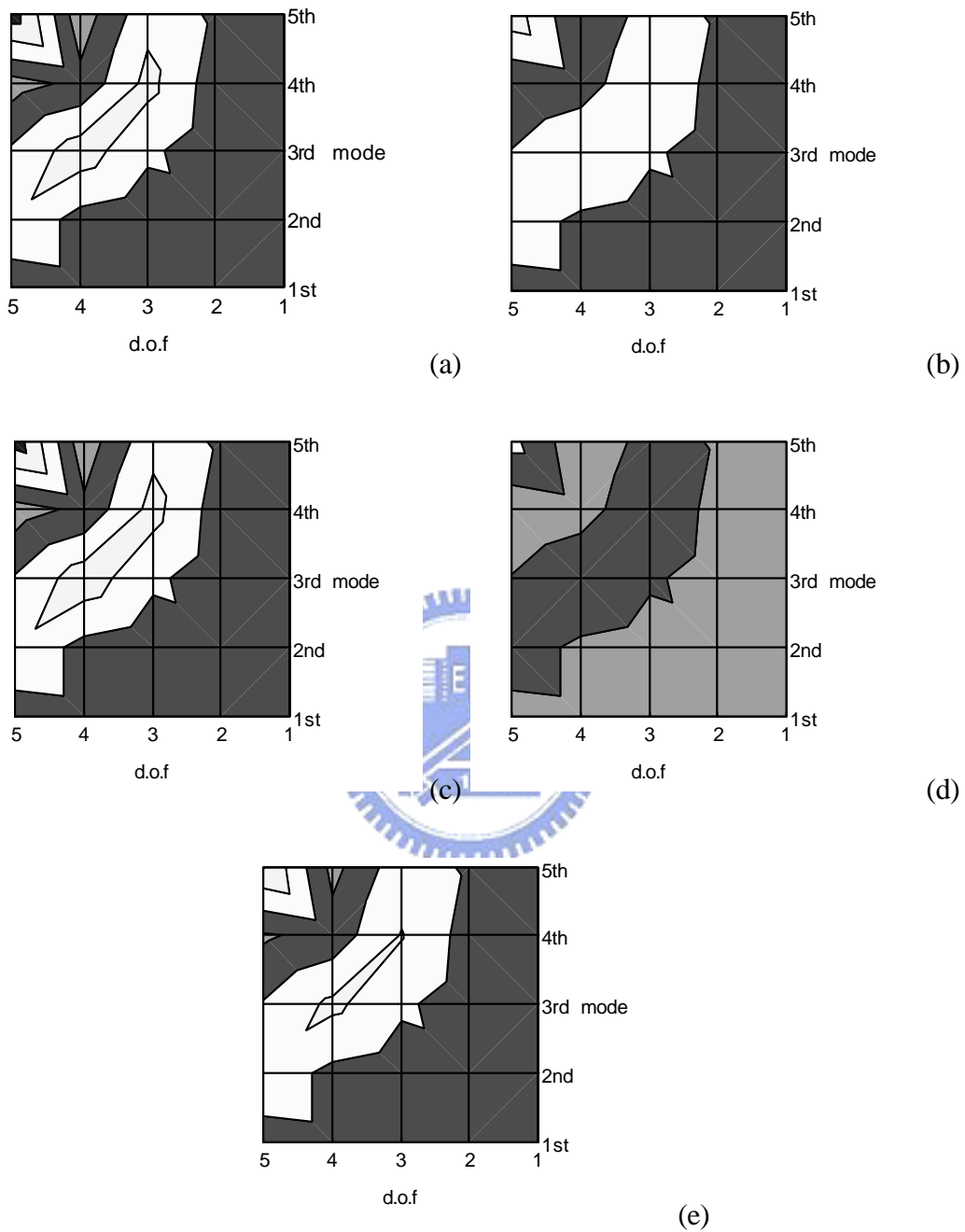
Figure 5.2 Plots of the DLF for the *Dam_k*₁ class with 26% damage extent

((a) to (e) are the plots of the DLF which are obtained by dividing the changes in the

modal vector to the changes in the 1st to 5th modal values, respectively)

Figure 5.3   Plots of the DLF for the *Dam_k*$_2$ class with 20% damage extent

((a) to (e) are the plots of the DLF which are obtained by dividing the changes in the

modal vector to the changes in the 1st to 5th modal values, respectively)

Figure 5.4 Plots of the DLF for the *Dam_k*$_3$ class with 20% damage extent

((a) to (e) are the plots of the DLF which are obtained by dividing the changes in the

modal vector to the changes in the 1st to 5th modal values, respectively)
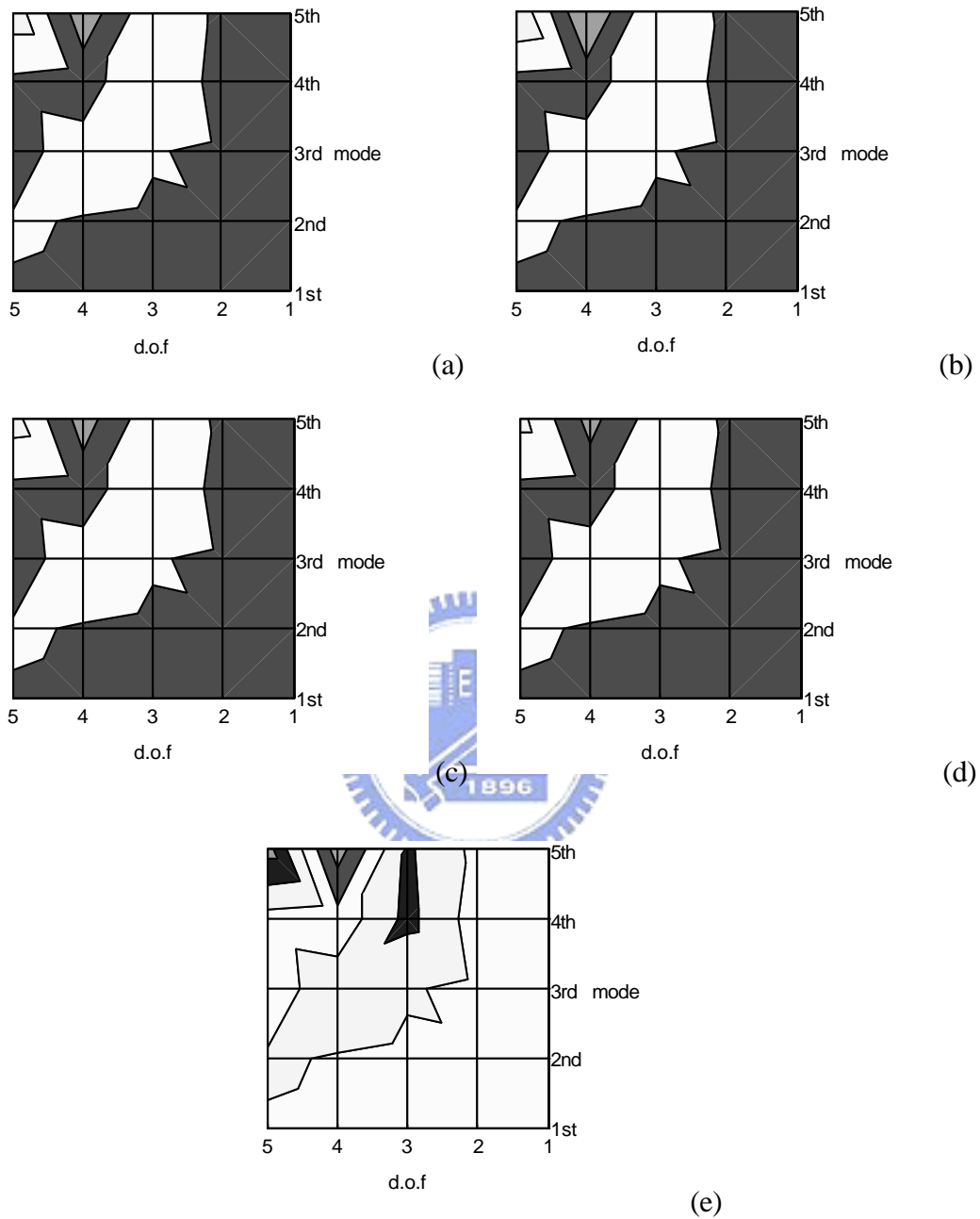
Figure 5.5 Plots of the DLF for the *Dam_k₁&k₂* class with 20% damage extent

((a) to (e) are the plots of the DLF which are obtained by dividing the changes in the

modal vector to the changes in the 1st to 5th modal values, respectively)

(a)

(b)

(c)

(d)

(e)
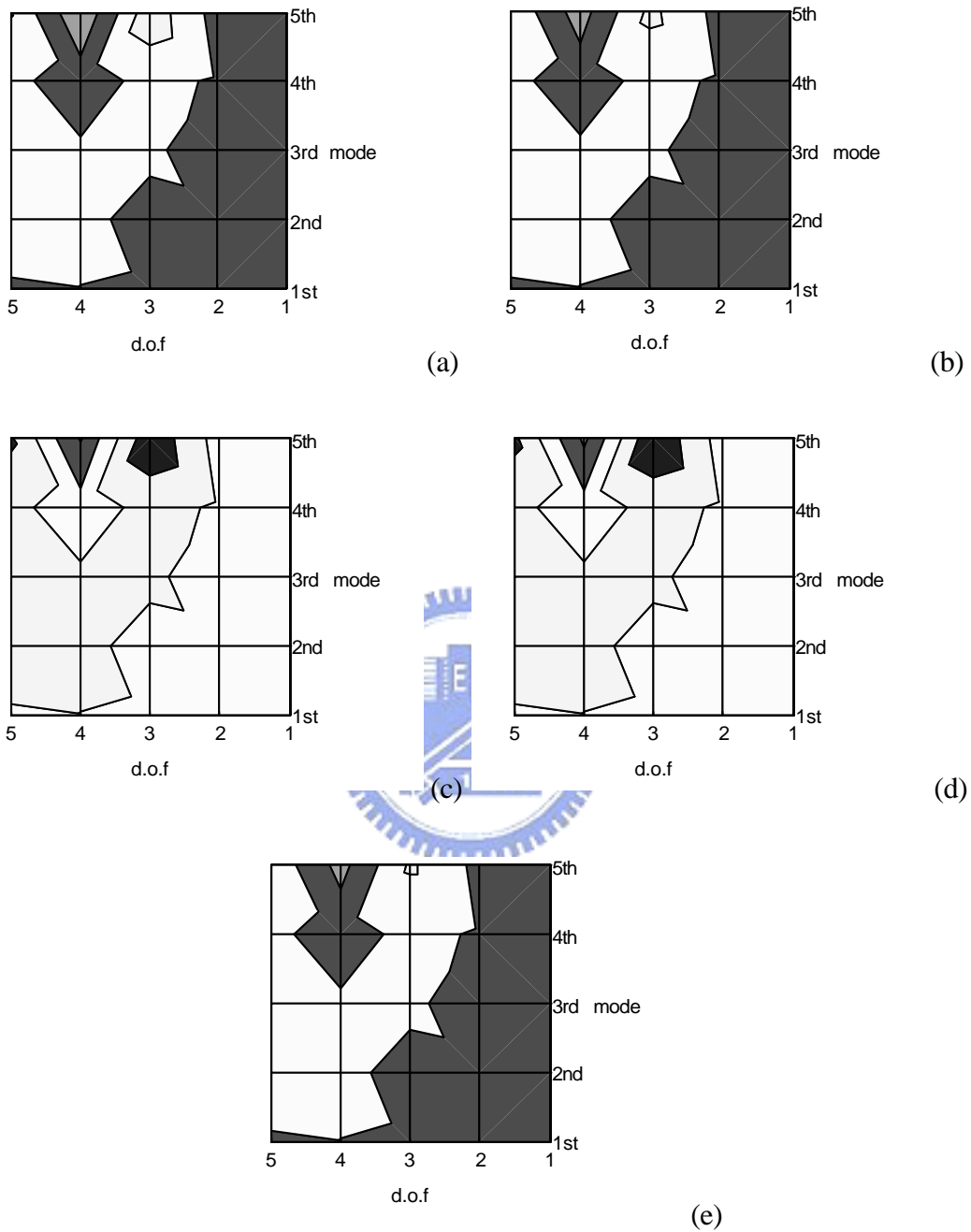
Figure 5.6   Plots of the DLF for the *Dam_k_1&k_3* class with 20% damage extent

((a) to (e) are the plots of the DLF which are obtained by dividing the changes in the

modal vector to the changes in the 1st to 5th modal values, respectively)

Training of the UFN

The ADLF together with the related structural element condition for each damage case is treated as an instance. Refer to Table 5.1, 132 instances are obtained. Note that, Case 1 to 10 are instances of damage class Dam_k_1; Case 21 to 40 are instances of damage class Dam_k_2; Case 41 to 60 are instances of damage class Dam_k_3; Case 61 to 96 are instances of damage class $Dam\_k_1\&k_2$; Case 97 to 132 are instances of damage class $Dam\_k_1\&k_3$. These 132 instances are separated into two sets: the training set and the testing set. For the UFN, the training set is also named as an instance base. Total of 18 instances that randomly selected from the 132 instances are collected as testing set to verify the performance of the UFN reasoning model. Table 5.2 lists some characterizations about the testing instances. Furthermore, the input values of the testing instances are treated as MDLF. Hence, the output of the testing instances will be generated through the UFN reasoning by matching the MDLF and ADLF.

Before verification of the testing instances, the UFN is trained first. The training of the UFN is to determine the upper bound R_{max} for the membership function and the weights a_m for the similarity measurement. According to Hung and Jan [85], an appropriate value of R_{max} is selected when the accumulative correlation coefficient (ACC) exceeds 0.8. Herein, the corresponding R_{max} that makes the accumulative correlation coefficient exceeds 0.85 is adopted for more strict. The value of R_{max} is determined to be 0.01 and the values of a_m are all set to be constant one.

Table 5.2 Characterizations of the testing instances

No. of instance	Output vector	Damage class	Damage severity (%)
1	[1, 0, 0]	Dam_k_1	8
2	[1, 0, 0]	Dam_k_1	26
3	[0, 1, 0]	Dam_k_2	6
4	[0, 1, 0]	Dam_k_2	22
5	[0, 0, 1]	Dam_k_3	12
6	[0, 0, 1]	Dam_k_3	24
7	[1, 1, 0]	$Dam\_k_1\&k_2$	5 & 10
8	[1, 1, 0]	$Dam\_k_1\&k_2$	10 & 10
9	[1, 1, 0]	$Dam\_k_1\&k_2$	15 & 10
10	[1, 1, 0]	$Dam\_k_1\&k_2$	20 & 20
11	[1, 1, 0]	$Dam\_k_1\&k_2$	25 & 15
12	[1, 1, 0]	$Dam\_k_1\&k_2$	30 & 20
13	[1, 0, 1]	$Dam\_k_1\&k_3$	5 & 15
14	[1, 0, 1]	$Dam\_k_1\&k_3$	10 & 15
15	[1, 0, 1]	$Dam\_k_1\&k_3$	15 & 20
16	[1, 0, 1]	$Dam\_k_1\&k_3$	20 & 10
17	[1, 0, 1]	$Dam\_k_1\&k_3$	25 & 25
18	[1, 0, 1]	$Dam\_k_1\&k_3$	30 & 15

Identification results without noise polluted in DLF

An index, *SDD* (Degree of Successful Diagnosis), is used to evaluate the accuracy of the predicted outputs of the networks. Herein, the values 0.2 and 0.8 are selected to be the threshold of the confirmed undamaged and damaged site, respectively. Restated, the generated output value of the network that less than 0.2 or larger than 0.8 is assumed to be a successful diagnosis for undamaged or damage case. The *SDD* is calculated by the following equation.

$$SDD = \frac{N_{SD}}{N_{ED}} \times 100\% \qquad (5.13)$$

where N_{SD} is the total number of the successful diagnosis; N_{ED} is the total number of the excepted diagnosis. The value *SDD* equals to 100% if the identifications of damage location(s) for all testing cases are correct; otherwise, a value 0% represents wrong damage localization happens to every testing cases.

Based on the working parameters generated from the training process, the verified results of the 18 testing instances are obtained and listed in Table 5.3. According to the verified results, the UFN reasoning model shows excellent agreement in localization of the damage (the *SDD* is 100%). It is interested to mention that, for testing instance 2, Cases 79 and 115 in the instance base are found to be 'similar' to this testing instance, even the damage class of the testing instance 2 (i.e. *Dam_k$_1$*) and those of Cases 79 and 115 (i.e. *Dam_k$_1$&k$_2$* and *Dam_k$_1$&k$_3$*, respectively) are different. However, the UFN reasoning model can still generates the correct result. Same situation also happens to the other testing instances such as testing instances 1, 9, 10, 11, 12, 13, 16, and 18.

Table 5.3 Diagnostic results via UFN (without noise)

No. of instance	True vector	UFN outputs	Similar instances
1	[1, 0, 0]	[1.00, 0.01, 0.02]	1,2,3,5,6,7,8,9,10,11,12,14,15,16,17,18,19,20,73, 79,80,85,86,91,92,93,95,115,121,127,128
2	[1, 0, 0]	[1.00, 0.00, 0.00]	1,2,3,5,6,7,8,9,10,11,12,14,15,16,17,18,19,20,79, 85,86,91,92,93,115,121,127,128
3	[0, 1, 0]	[0.00, 1.00, 0.00]	21,22,24,25
4	[0, 1, 0]	[0.00, 1.00, 0.00]	28,29,30,32,33,34,35
5	[0, 0, 1]	[0.00, 0.00, 1.00]	41,42,43,44,45,47,48,49,50,51,52
6	[0, 0, 1]	[0.00, 0.00, 1.00]	47,48,49,50,51,52,53,54,56,57,58
7	[1, 1, 0]	[1.00, 1.00, 0.00]	61,63,64,65,69,70,71,72
8	[1, 1, 0]	[1.00, 1.00, 0.00]	61,67,69,70,71,72,75,76,77,78,80,81,83,84,88,89, 90,95,96
9	[1, 1, 0]	[1.00, 0.99, 0.00]	61,67,69,70,71,72,73,75,76,77,78,79,80,81,83,84, 85,86,88,89,90,92,93,95,96,103,109,116,122
10	[1, 1, 0]	[1.00, 1.00, 0.00]	61,67,69,70,71,72,73,75,76,77,78,79,80,81,83,84, 85,86,88,89,90,92,93,95,96,109
11	[1, 1, 0]	[1.00, 0.99, 0.01]	1,2,3,5,6,67,73,75,76,77,79,80,81,83,84,85,88,89, 92,93,95,96,103,109,115,121,122,127,128
12	[1, 1, 0]	[1.00, 0.98, 0.02]	1,2,3,6,7,9,10,67,73,75,76,77,79,80,81,83,84,85, 86,89,90,91,92,95,96,109,115,121,122,127,128
13	[1, 0, 1]	[0.99, 0.00, 1.00]	56,57,58,59,98,100,101,102,106,107,108
14	[1, 0, 1]	[1.00, 0.00, 1.00]	97,98,104,106,107,108,111,113,114,118,119,120, 126
15	[1, 0, 1]	[1.00, 0.00, 1.00]	97,98,104,106,107,108,110,111,113,114,117,118, 119,120,124,126,131,132
16	[1, 0, 1]	[1.00, 0.01, 0.99]	67,73,79,80,81,86,92,93,103,104,109,110,115,117, 118,121,122,123,126,127,128,130,131,132
17	[1, 0, 1]	[1.00, 0.00, 1.00]	97,103,104,110,111,113,114,117,118,119,120,122, 123,124,126,130,131,132
18	[1, 0, 1]	[1.00, 0.02, 0.98]	67,73,79,80,85,86,91,92,93,103,109,110,115,117, 118,121,122,123,124,127,128,130,131,132

Because the upper bound R_{max} is selected when the accumulative correlation coefficient exceeds 0.85, an explanation is made that the found similar instances have more than 85% correlation with the testing instance. Restated, when the solution for a testing instance is obtained through the UFN, the degree of reliability of the solved solution is more than 85%. Consequently, the output values of the UFN have a further meaning. For example, the output vector for the testing instance 18 is [1.00, 0.02, 0.98] which means that the possibilities of the elemental damage are 100%, 2%, and 98%, respectively, based on the reliability of 85%.

Verified results with noise polluted in DLF

In practical situations, there are always differences between the analytical model and actual structure, and the measurements are usually noise contaminated. Consequently, it is impossible that the measured modal parameters are identical to the analytical ones. In order to make the proposed damage detection method more practical, the noise effect is considered in the verification. In this study, the mode shapes are noise polluted with various levels of random signals. The contaminated signal is represented in s simple way as [25]

$$\bar{\boldsymbol{f}}_{ij} = \boldsymbol{f}_{ij}(1 + r_i^f l^f \mid \boldsymbol{f}_{\text{max}, j} \mid) \tag{5.14}$$

where $\bar{\boldsymbol{f}}_{ij}$ and $\boldsymbol{f}_{ij}$ are the mode shape components of the jth mode at the ith DOF with and without noise, respectively; r_i^f is the random number with zero mean and unit variance; l^f is the noise level; and $\boldsymbol{f}_{\text{max}, j}$ is the largest component in the jth mode shape.

Table 5.4 shows the diagnostic results of the testing instances of which the mode shapes are contaminated with 1%, 3%, and 4% random noise, respectively. As mentioned previously, the values 0.2 and 0.8 are used to be the threshold of the confirmed undamaged and damaged site. The UFN outputs, listed in Table 5.4, also show the correct diagnosis about the damage location except for the testing instance 3 with 4% contaminated noise. The *SDD* for the 1% and 3% measured noise conditions are both 100%, and the *SDD* for the 4% measured noise condition can still reach 94.4%. The reason why the UFN can not generate an output vector in the condition of 4% measured noise is that the matching process finds no similar instances in the instance base within 85% degree of correlation. To overcome this problem, two strategies are employed in this work. One is to loose the degree of correlation (i.e. to select a larger value of R_{max}). The other is to select the instance with the smallest degree of difference as the similar instance to generate the output vector. For example, if the second strategy is adopted, the output vector of the unsolved testing instance 3 will be [0.00, 1.00, 0.00], and the *SDD* would be 100% which means the identifications of the damage locations are undoubtedly successful.

Table 5.4 Diagnostic results via UFN (with various noise levels)

No. of instance	UFN output vector		
	1% noise	3% noise	4% noise
1	[1.00, 0.08, 0.04]	[1.00, 0.11, 0.01]	[1.00, 0.19, 0.04]
2	[1.00, 0.01, 0.00]	[1.00, 0.01, 0.01]	[1.00, 0.04, 0.02]
3	[0.00, 1.00, 0.00]	[0.00, 1.00, 0.00]	[NA, NA, NA] ([0.00, 1.00, 0.00])[#]
4	[0.00, 1.00, 0.00]	[0.00, 1.00, 0.00]	[0.00, 1.00, 0.00]
5	[0.00, 0.00, 1.00]	[0.00, 0.00, 1.00]	[0.00, 0.00, 1.00]
6	[0.00, 0.00, 1.00]	[0.00, 0.00, 1.00]	[0.04, 0.00, 1.00]
7	[1.00, 1.00, 0.00]	[1.00, 1.00, 0.00]	[1.00, 1.00, 0.00]
8	[1.00, 1.00, 0.00]	[1.00, 1.00, 0.00]	[1.00, 1.00, 0.00]
9	[1.00, 1.00, 0.00]	[1.00, 0.99, 0.00]	[1.00, 1.00, 0.00]
10	[1.00, 1.00, 0.00]	[1.00, 1.00, 0.00]	[1.00, 1.00, 0.00]
11	[1.00, 0.99, 0.01]	[1.00, 0.98, 0.02]	[1.00, 0.98, 0.02]
12	[1.00, 0.98, 0.02]	[1.00, 0.97, 0.02]	[1.00, 0.98, 0.01]
13	[0.99, 0.00, 1.00]	[0.99, 0.00, 1.00]	[0.87, 0.00, 1.00]
14	[1.00, 0.00, 1.00]	[1.00, 0.00, 1.00]	[1.00, 0.00, 1.00]
15	[1.00, 0.00, 1.00]	[1.00, 0.00, 1.00]	[1.00, 0.00, 1.00]
16	[1.00, 0.01, 0.99]	[1.00, 0.01, 0.99]	[1.00, 0.03, 0.97]
17	[1.00, 0.00, 1.00]	[1.00, 0.00, 1.00]	[1.00, 0.00, 1.00]
18	[1.00, 0.02, 0.98]	[1.00, 0.02, 0.98]	[1.00, 0.03, 0.97]
SDD	100%	100%	94.4%

Note: NA: data not available. (finds no similar instance)

 #: when the most similar instance is chosen

Verified results while using the incomplete modal data

Usually, only a truncated set of modal data can be obtained experimentally. Besides, only partial DOF with respect to the total DOF of a real structural would be monitored (especially for civil engineering structures), which results in the incomplete measured mode shapes. Therefore, the effect of using incomplete modal data (truncated set of modal frequencies and incomplete mode shapes) is investigated to testing the robustness of the UFN in damage detection. Assumed that only the 1st, 2nd, and 3rd mode can be obtained and only the 1st, 3rd, and 5th DOF of the structure are monitored. Hence, the number of the input variables is substantially reduced from 100 to 18. Table 5.5 shows the verified results of the UFN in damage detection while using the incomplete modal data with/without noise. It is clear from the table that, even with the measured noise and partial modal data, the UFN still can locate the damaged sites satisfactorily. The *SDD* for the conditions of 0%, 1%, and 3% measured noise are 100%, 100%, and 94.4%, respectively. The results shown here validate that the proposed damage detection approach is robust and flexible when dealing with the measured noise and (or) incomplete modal data situations.

Table 5.5 Diagnostic results of using incomplete modal data via UFN

No. of instance	UFN output vector		
	without noise	1% noise	3% noise
1	[1.00, 0.01, 0.04]	[1.00, 0.13, 0.07]	[1.00, 0.16, 0.12]
2	[1.00, 0.00, 0.00]	[1.00, 0.02, 0.02]	[1.00, 0.08, 0.03]
3	[0.00, 1.00, 0.00]	[0.00, 1.00, 0.00]	[NA, NA, NA] ([0.00, 1.00, 0.00])[#]
4	[0.00, 1.00, 0.00]	[0.00, 1.00, 0.00]	[0.00, 1.00, 0.00]
5	[0.00, 0.00, 1.00]	[0.00, 0.00, 1.00]	[0.03, 0.00, 1.00]
6	[0.00, 0.00, 1.00]	[0.01, 0.00, 1.00]	[0.01, 0.00, 1.00]
7	[1.00, 1.00, 0.00]	[1.00, 1.00, 0.00]	[1.00, 1.00, 0.00]
8	[1.00, 1.00, 0.00]	[1.00, 1.00, 0.00]	[1.00, 1.00, 0.00]
9	[1.00, 0.99, 0.00]	[1.00, 0.99, 0.00]	[0.98, 1.00, 0.00]
10	[1.00, 1.00, 0.00]	[1.00, 1.00, 0.00]	[1.00, 1.00, 0.00]
11	[1.00, 0.98, 0.00]	[1.00, 0.97, 0.00]	[1.00, 0.99, 0.00]
12	[1.00, 0.98, 0.00]	[1.00, 0.97, 0.00]	[1.00, 1.00, 0.00]
13	[0.94, 0.00, 1.00]	[0.94, 0.00, 1.00]	[0.92, 0.00, 1.00]
14	[1.00, 0.00, 1.00]	[1.00, 0.00, 1.00]	[1.00, 0.00, 1.00]
15	[1.00, 0.00, 1.00]	[1.00, 0.00, 1.00]	[1.00, 0.00, 1.00]
16	[1.00, 0.00, 0.96]	[1.00, 0.00, 0.94]	[1.00, 0.00, 0.96]
17	[1.00, 0.00, 1.00]	[1.00, 0.00, 1.00]	[1.00, 0.00, 1.00]
18	[1.00, 0.00, 0.94]	[1.00, 0.00, 0.94]	[1.00, 0.00, 0.90]
SDD	100%	100%	94.4% (100%)[#]

Note: NA: data not available. (finds no similar instance)
    #: when the most similar instance is chosen for NA situation

__Compare with the BPN__

In this example, the same data set is also process through a supervised neural network for the sake of comparison. A backpropagation network (BPN) with the topology of (100-53-3) is adopted. The training is terminated when the system error of the BPN is smaller than that of the UFN. The diagnostic results of the instances without and with noise are listed in Table 5.5. It is evident that the BPN can precisely detect the location of the damaged element when the data set is not polluted. However, even with small intensity of noise (with 1% noise), the BPN could possibly generate the incorrect damage localization. For example, the BPN outputs for the testing instance 1 indicate that the damage occurred at the 1st and 3rd story columns, while the actual damage occurred at the 1st story columns only. According to the numerical example, although the system error of the network output for BPN is slightly smaller than that for UFN, it is important to mention that BPN is more inflexible due to the possibility of incorrect diagnosis when dealing with measured noise. Even though, it is clear from this study and other researches that neural network is a promising technique in damage detection of structures.

Table 5.6 Diagnostic results via BPN

No. of instance	BPN output vector	
	without noise	1% noise
1	[1.00, 0.00, 0.00]	[1.00, 0.00, 0.44*]
2	[1.00, 0.00, 0.00]	[1.00, 0.00, 0.00]
3	[0.00, 1.00, 0.00]	[0.00, 1.00, 0.00]
4	[0.00, 1.00, 0.00]	[0.00, 1.00, 0.00]
5	[0.00, 0.00, 1.00]	[0.00, 0.00, 1.00]
6	[0.00, 0.00, 1.00]	[0.00, 0.00, 1.00]
7	[1.00, 1.00, 0.01]	[1.00, 1.00, 0.00]
8	[1.00, 1.00, 0.00]	[1.00, 1.00, 0.00]
9	[1.00, 1.00, 0.00]	[1.00, 1.00, 0.00]
10	[1.00, 1.00, 0.00]	[1.00, 1.00, 0.00]
11	[1.00, 1.00, 0.00]	[1.00, 1.00, 0.00]
12	[1.00, 1.00, 0.00]	[1.00, 1.00, 0.00]
13	[1.00, 0.00, 1.00]	[1.00, 0.00, 1.00]
14	[1.00, 0.01, 1.00]	[1.00, 0.00, 1.00]
15	[1.00, 0.00, 1.00]	[1.00, 0.00, 1.00]
16	[1.00, 0.00, 1.00]	[1.00, 0.00, 1.00]
17	[1.00, 0.00, 1.00]	[1.00, 0.00, 1.00]
18	[1.00, 0.00, 1.00]	[1.00, 0.00, 1.00]
SDD	100%	98.1%

Note: The value with the notation '*' means wrong diagnosis.

5.3   Estimation Of Damage Extent

After the possible damage locations were identified via damage localization procedure, the damage extent for each damage location can be assessed by the estimation algorithms. Almost all of the proposed estimation algorithms of damage extent in previous works, such as Kaouk and Zimmermann [43], Stubbs and Kim [29], Messina *et al.* [31, 32], Shi *et al.* [24, 25, 33, 45, 101], and Law *et al.* [102], rely on an analytical model for the real structural system to provide certain basic information, such as modal mass and elemental stiffness matrix. Based on the analytical model, the estimation algorithms can be employed to assess the structural damage extent. Herein, a simple approach for assessing the damage extent is introduced as follow.

5.3.1   Algorithms for the Estimation of Damage Extent

Begin from equation (5.2) and rewrite it down here.

$$[(\mathbf{K} - \Delta \mathbf{K}) - (l_i - \Delta l_i)\mathbf{M}](\boldsymbol{f}_i - \Delta \boldsymbol{f}_i) = 0 \qquad (5.2)$$

Expand this equation and then pre-multiply with $\boldsymbol{f}_i^T$ yields

$$-\boldsymbol{f}_i^T \Delta \mathbf{K} \boldsymbol{f}_i + \Delta l_i \boldsymbol{f}_i^T \mathbf{M} \boldsymbol{f}_i - \boldsymbol{f}_i^T \Delta \mathbf{K} \Delta \boldsymbol{f}_i + \Delta l_i \boldsymbol{f}_i^T \mathbf{M} \Delta \boldsymbol{f}_i = 0 \qquad (5.15)$$

After imposed equation (5.3) on (5.15) and rearranged, equation (5.15) becomes

$$\Delta l_i = \frac{\boldsymbol{f}_i^T \displaystyle\sum_{e=1}^{N_d} a_e \mathbf{k}_e (\boldsymbol{f}_i - \Delta \boldsymbol{f}_i)}{\boldsymbol{f}_i^T \mathbf{M}(\boldsymbol{f}_i - \Delta \boldsymbol{f}_i)} = \frac{\boldsymbol{f}_i^T \displaystyle\sum_{e=1}^{N_d} a_e \mathbf{k}_e \boldsymbol{f}_{di}}{\boldsymbol{f}_i^T \mathbf{M} \boldsymbol{f}_{di}} \qquad (5.16)$$

where $\boldsymbol{f}_{di} = \boldsymbol{f}_i - \Delta \boldsymbol{f}_i$ is the ith mode shape after the structure was damaged. Note

that, if the higher order terms of Δ were neglected, equation (5.15) leads to equation (5.6). Furthermore, if the mode shape of the damaged structure, $\boldsymbol{f}_{di}$, is replaced by the mode shape of the undamaged structure, $\boldsymbol{f}_i$, equation (5.16) becomes equation (5.6)

Expand the above equation yields

$$\Delta l_i = \frac{\boldsymbol{f}_i^T (\boldsymbol{a}_1 \mathbf{k}_1 + \boldsymbol{a}_2 \mathbf{k}_2 + \cdots + \boldsymbol{a}_{N_d} \mathbf{k}_{N_d}) \boldsymbol{f}_{di}}{\boldsymbol{f}_i^T \mathbf{M} \boldsymbol{f}_{di}}$$

$$= \left[\frac{\boldsymbol{f}_i^T \mathbf{k}_1 \boldsymbol{f}_{di}}{\boldsymbol{f}_i^T \mathbf{M} \boldsymbol{f}_{di}} \quad \frac{\boldsymbol{f}_i^T \mathbf{k}_2 \boldsymbol{f}_{di}}{\boldsymbol{f}_i^T \mathbf{M} \boldsymbol{f}_{di}} \quad \cdots \quad \frac{\boldsymbol{f}_i^T \mathbf{k}_{N_d} \boldsymbol{f}_{di}}{\boldsymbol{f}_i^T \mathbf{M} \boldsymbol{f}_{di}} \right] \begin{Bmatrix} \boldsymbol{a}_1 \\ \boldsymbol{a}_2 \\ \vdots \\ \boldsymbol{a}_{N_d} \end{Bmatrix} \qquad (5.17.\text{a})$$

$$= \begin{bmatrix} A_{i1}^* & A_{i2}^* & \cdots & A_{iN_d}^* \end{bmatrix} \{\boldsymbol{a}\}$$

$$= \sum_{j=1}^{N_d} A_{ij}^* \boldsymbol{a}_j$$

where i and j represent the ith modal data and the jth identified damage location, respectively, and $A_{ij}^* = \dfrac{\boldsymbol{f}_i^T \mathbf{k}_j \boldsymbol{f}_{di}}{\boldsymbol{f}_i^T \mathbf{M} \boldsymbol{f}_{di}}$. If equation (5.6) is expanded, a similar form to equation (5.17.a) is yielded

$$\Delta l_i = \begin{bmatrix} A_{i1} & A_{i1} & \cdots & A_{iN_d} \end{bmatrix} \{\boldsymbol{a}\}$$

$$= \sum_{j=1}^{N_d} A_{ij} \boldsymbol{a}_j \qquad (5.17.\text{b})$$

where $A_{ij} = \dfrac{\boldsymbol{f}_i^T \mathbf{k}_j \boldsymbol{f}_i}{\boldsymbol{f}_i^T \mathbf{M} \boldsymbol{f}_i}$.

In applications, two sets of data, model-based and measurement-based data are needed when equation (5.17) is employed to estimate the damage extent. The model-based data are the analytical modal mass, $\mathbf{M}$, and the elemental stiffness

matrix, $\mathbf{k}_e$. The measurement-based data are the changes of modal values, Δl_i, and the mode shapes of the undamaged and damaged structure, $\boldsymbol{f}_i$ and $\boldsymbol{f}_{di}$, respectively. In the case of all the measurement-based data are available, both equations (5.17.a) and (5.17.b) can be employed; while only changes of modal values are obtained, equation (5.17.b) is adopted. Theoretically, if the analytical model quite approximates to the real structure and the structural mode shapes are correctly extracted from the measurements, using equation (5.17.a) results in more accurate estimation of the damage extent. However, these two hypotheses are usually difficult to be accomplished. As known, the estimation of experimental modal shapes is not as accurate as that of modal frequencies. Consequently, equation (5.17.b) may be the better alternative when estimating the damage extent of a real structure in order to avoid including too much imprecise data.

Look back to equations (5.17.a) and (5.17.b), if N modal data are provided, they are extended to

$$\{\Delta l\} = \mathbf{A}^*\{a\} \tag{5.18.a}$$

$$\{\Delta l\} = \mathbf{A}\{a\} \tag{5.18.b}$$

where $\mathbf{A}^*$ and $\mathbf{A}$ are matrixes with $N \times N_d$ entries.

By means of the least-square method, the damage extent, $\{a\}$, can be estimated from equation (5.18). Take equation (5.18.b) for example, for the number of equations equal to the number of unknowns (i.e. $N = N_d$),

$$\{a\} = \mathbf{A}^{-1}\{\Delta l\} \tag{5.19.a}$$

or the number of equations greater than the number of unknowns (i.e. $N > N_d$),

$$\{a\} = (\mathbf{A}^T \mathbf{A})^{-1} \mathbf{A}^T \{\Delta l\} \qquad\qquad (5.19.b)$$

For the number of equations smaller than the number of unknowns (i.e. $N < N_d$),

$$\{a\} = \mathbf{A}^T (\mathbf{A}\mathbf{A}^T)^{-1} \{\Delta l\} \qquad\qquad (5.19.c)$$

Note that, one of the reasons of using two-stage damage assessment methods is that the number of unknowns could be reduced after the damage locations were identified in the first stage of damage assessment. Therefore, equation (5.19.c) would be seldom used in most cases; meanwhile, equations (5.19.a) and (5.19.b) give satisfactory assessment of the structural damage extent. For the worst condition in which the number of equations quite smaller than the number of unknowns, equation (5.19.c) may lead to incorrect answer. To solve this problem, equation (5.11) can be used as supplement to increase the number of equations.
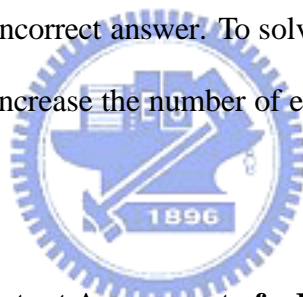
5.3.2   Example   Damage Extent Assessment of a Five-Story Shear Frame

To continue the example presented in section 5.2.4, the damage extents for each damage case listed in Table 5.2 is evaluated using equation (5.19) based on the identified damage location(s). Two circumstances are discussed here: the first one is that the measured modal shapes are assumed to be noise-free (the identifications of damage location via UFN were listed in Table 5.3); and the second one further considers of using contaminated modal shapes with 3% noise (the identifications of damage location via UFN were listed in Table 5.4). The results of assessing the damage extents for each damage case under two discussed circumstances are listed in Tables 5.7 and 5.8, respectively. For comparison, the values of damage extent are diagrammatically illustrated in Figures 5.7 and 5.8 which refer to Tables 5.7 and 5.8,

respectively. Based on the estimated results, several appearances are discovered and discussed below.

(1)   According to Table 5.7, the estimated values of damage extent when using equation (5.18.a) are identical to the exact ones. This phenomenon is easy to interpret based on the facts that the higher order terms of Δ were not eliminated when deriving equation (5.18.a) and the mode shapes used in generating $\mathbf{A}^*$ matrix are noise-free. On the other hand, the assessed values of damage extent when using equation (5.18.b) differ from the exact ones. With larger damage extent, the difference between estimations and exact values became larger.

(2)   Both the estimated results (Tables 5.7 and 5.8) indicated that the algorithms for assessing the damage extent yield satisfactory estimation even the mode shapes were noise-polluted.

(3)   The damage extent is overestimated in most damage cases when equation (5.18.b) was adopted. This may resulted from that the influence of the higher order terms of Δ became noticeable with increasing damage extent. Therefore, from the view of practice, equation (5.18.b) seems to be a better alternative for the sake of conservation.

Table 5.7 Estimation of the damage extent based on the localization results

in Table 5.3

No. of instance	Identified damage location	Damage extent (%)		
		Exact	Estimated (5.18.a)	Estimated (5.18.b)
1	k_1	8	8	8.47
2	k_1	26	26	31.70
3	k_2	6	6	6.27
4	k_2	22	22	26.15
5	k_3	12	12	13.33
6	k_3	24	24	29.95
7	k_1 & k_2	5 & 10	5 & 10	4.94 & 10.68
8	k_1 & k_2	10 & 10	10 & 10	10.11 & 10.73
9	k_1 & k_2	15 & 10	15 & 10	15.53 & 10.97
10	k_1 & k_2	20 & 20	20 & 20	20.51 & 22.93
11	k_1 & k_2	25 & 15	25 & 15	26.78 & 17.49
12	k_1 & k_2	30 & 20	30 & 20	32.51 & 23.87
13	k_1 & k_3	5 & 15	5 & 15	6.62 & 13.98
14	k_1 & k_3	10 & 15	10 & 15	13.01 & 11.85
15	k_1 & k_3	15 & 20	15 & 20	21.27 & 13.20
16	k_1 & k_3	20 & 10	20 & 10	23.73 & 8.14
17	k_1 & k_3	25 & 25	25 & 25	38.43 & 10.59
18	k_1 & k_3	30 & 15	30 & 15	38.33 & 11.60

Table 5.8 Estimation of the damage extent based on the use of noise-polluted

mode shapes and the localization results in Table 5.4

No. of instance	Identified damage location	Damage extent (%)		
		Exact	Estimated (5.19.a)	Estimated (5.19.b)
1	k_1	8	7.93	8.31
2	k_1	26	25.59	31.82
3	k_2	6	6.29	6.66
4	k_2	22	22.03	24.98
5	k_3	12	12.50	14.50
6	k_3	24	25.75	30.19
7	k_1 & k_2	5 & 10	4.97 & 9.53	4.92 & 9.79
8	k_1 & k_2	10 & 10	10.28 & 9.05	10.31 & 10.20
9	k_1 & k_2	15 & 10	15.11 & 10.04	15.16 & 11.63
10	k_1 & k_2	20 & 20	19.83 & 19.69	20.12 & 24.00
11	k_1 & k_2	25 & 15	24.62 & 15.18	26.79 & 18.59
12	k_1 & k_2	30 & 20	29.88 & 20.50	32.40 & 24.25
13	k_1 & k_3	5 & 15	6.13 & 12.35	8.02 & 10.33
14	k_1 & k_3	10 & 15	10.20 & 14.01	10.03 & 19.44
15	k_1 & k_3	15 & 20	15.80 & 20.64	19.51 & 17.73
16	k_1 & k_3	20 & 10	18.22 & 15.21	22.56 & 11.75
17	k_1 & k_3	25 & 25	25.81 & 26.84	38.39 & 10.31
18	k_1 & k_3	30 & 15	30.81 & 14.93	39.60 & 11.67
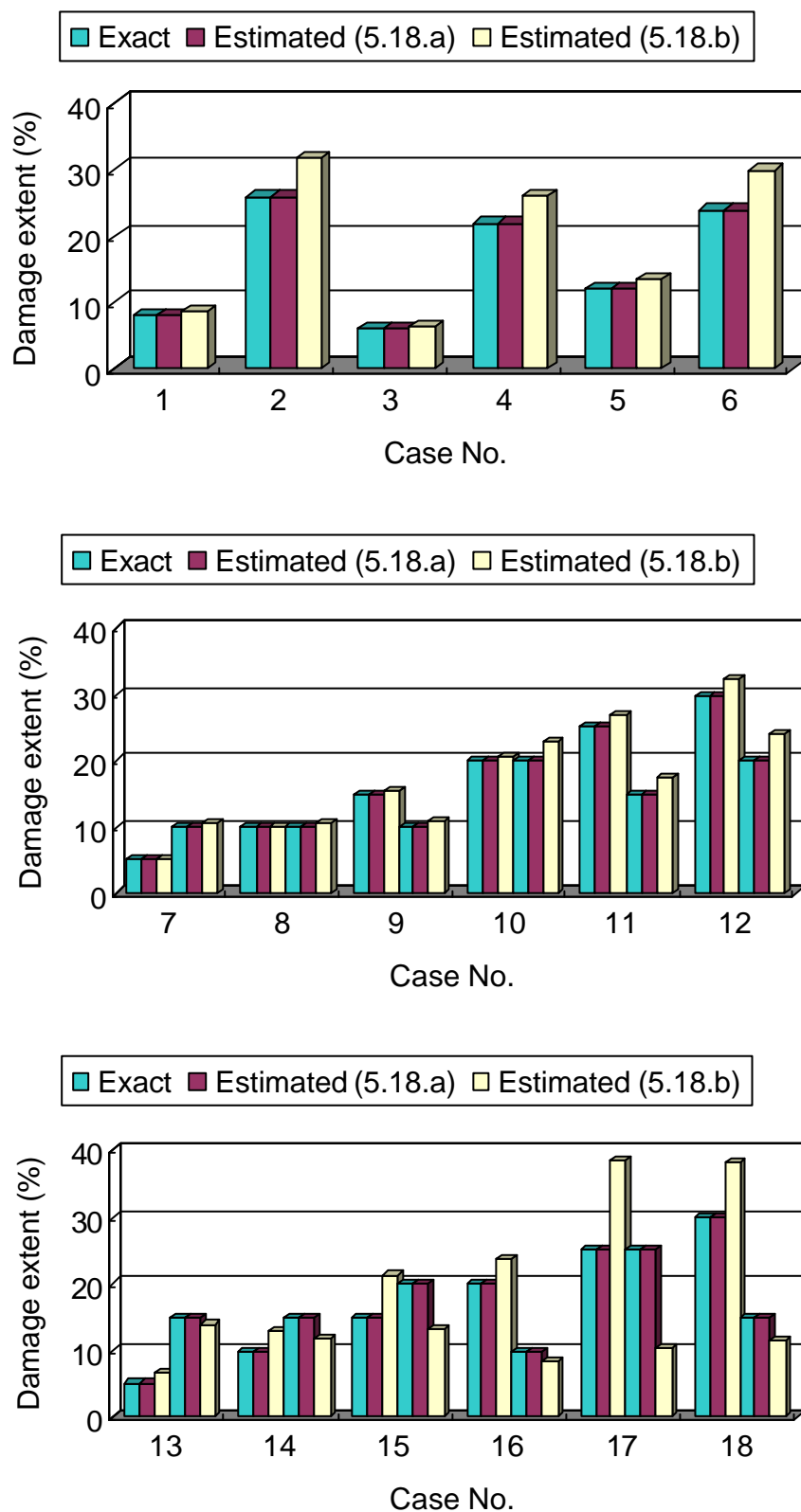
Figure 5.7 Estimations of the damage extent using noise-free modal data
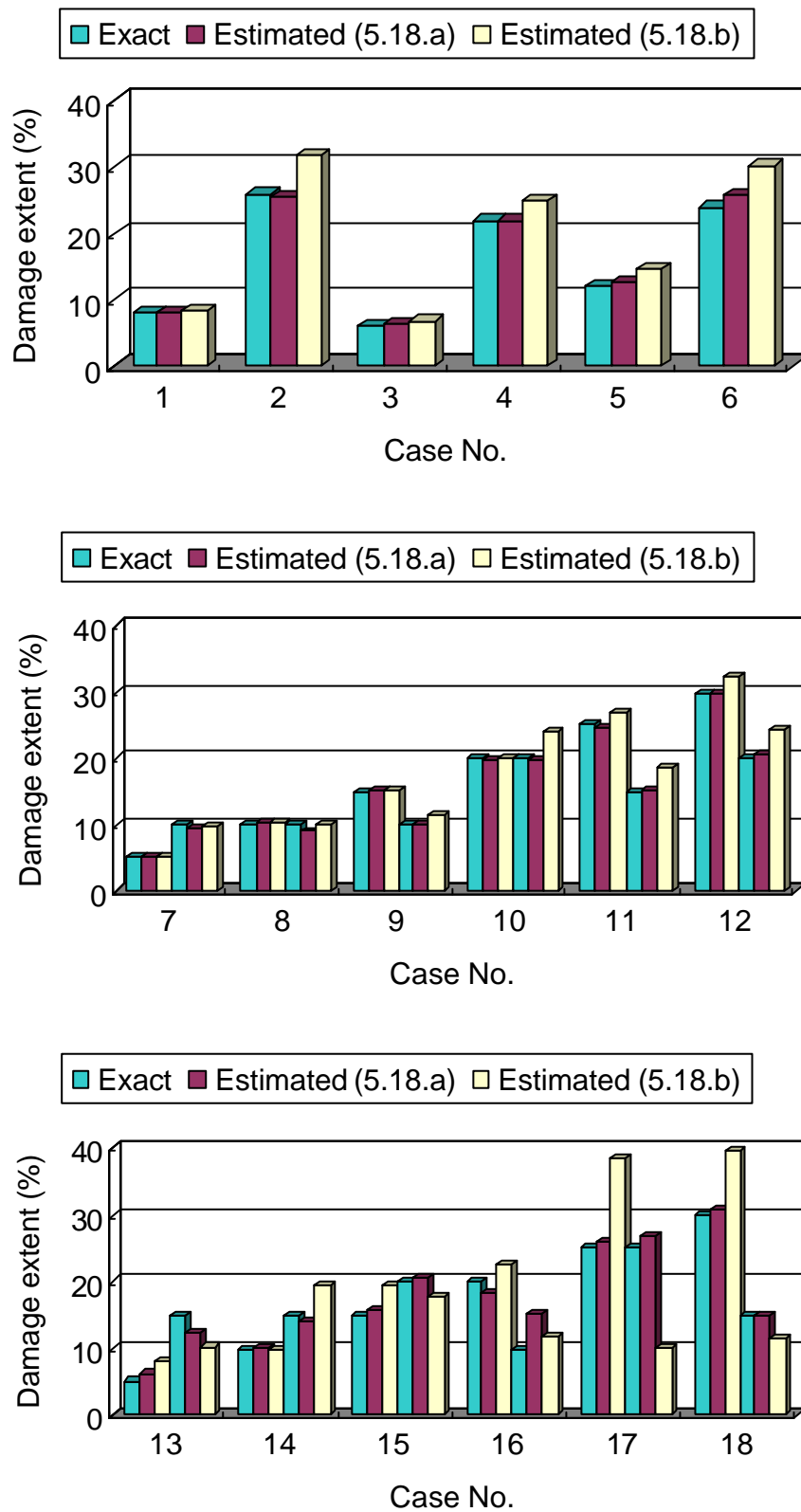
Figure 5.8 Estimations of the damage extent using noise-polluted modal data